A Hybrid ZVS Resonant Converter with Reduced Circulating Current and Improved Voltage Regulation Performance

Haoyu Wang, *Member, IEEE*

School of Information Science and Technology
ShanghaiTech University, Shanghai, China, 200031
Email: wanghy@shanghaitech.edu.cn

***Abstract*— In this paper, a novel hybrid ZVS resonant topology is proposed for PEV battery charging applications. The proposed charger architecture combines the advantages of SRC and LLC topologies while avoids their drawbacks in battery charging application. The circulating current in the magnetizing inductor is reduced, which helps to reduce the circulating losses. The peak current of primary MOSFETs are also reduced in comparison to the conventional LLC topology; this reduces the conduction losses from the MOSFETs and improves the circuit reliability. Moreover, turning off current of power MOSFETs are reduced, which reduces the switching losses associated with the turning off of MOSFETs. Simulation results based on designed 1 kW prototype shows 96.8% peak conversion efficiency.**

Keywords*— *battery charging, LLC, plug-in electric vehicle (PEV), series resonat converter (SRC), zero voltage switching (ZVS).

I. INTRODUCTION

In comparison to conventional pulse width modulation (PWM) converters, frequency modulated resonant converters exhibit advantages such as (a) reduced switching losses and thus higher conversion efficiency, (b) capability to operate at higher switching frequencies, which helps to reduce the size of magnetic components and thus to improve the power density, and (c) wide zero-voltage switching (ZVS) range, which can eliminate turning-off losses of body diodes, turning-on losses of MOSFETs, and some sources of electromagnetic interference (EMI) [1]–[4]. The block diagram of conventional resonant dc/dc converter is presented in Fig. 1. A single resonant converter consists of five parts: (a) a dc voltage source and switch network, which operate as a square wave generator, (b) a resonant tank, (c) a high frequency transformer, (d) rectifier, and (e) a low pass filter [5]–[7].

Based on the differences in the resonant tank and its relationship with the load, resonant dc/dc topologies are classified into four categories, (a) series resonant converter (SRC), (b) parallel resonant converter (PRC), (c) LCC series-parallel resonant converter (LCC), and (d) LLC series-parallel resonant converter (LLC). Fig. 2. Illustrates those four types of resonant tank networks.

In variety of battery charging systems, the battery voltage and load condition vary in a wide range depending on the different state of charge of the battery, as well as different battery types [8]. Therefore, operating with maximum

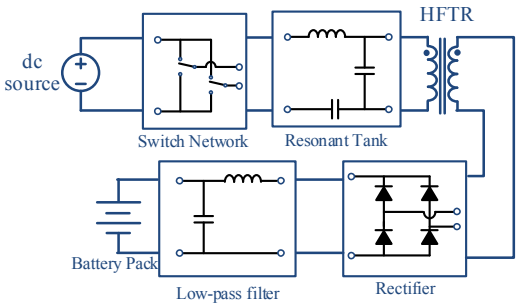

Fig. 1. Block diagram of a conventional resonant dc/dc converter.

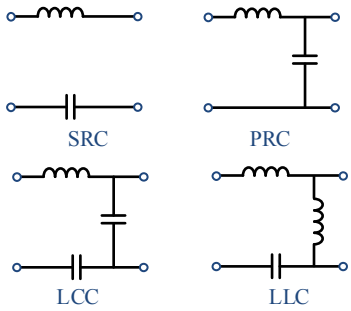

Fig. 2. Four most common typical resonant tank networks.

efficiency through reducing the conduction and switching losses over the full output voltage and load ranges is a challenging issue in isolated resonant charger design [9].

For resonant converters, circulating energy in the resonant tank is a significant figure of merit to evaluate the conduction losses[10]. Higher circulating energy corresponds to higher conductions losses and lower conversion efficiency [11]–[13].

SRC is one of the most classic resonant topologies. It has low circulating current in the resonant tank at high state of charge (SOC) [14]–[16]. However, the critical defect of SRC lies in its unacceptable poor voltage regulation performance in light load condition [11], [17]. Moreover, with switching frequency higher than the resonant frequency of the resonant tank, SRC circuit operates in continuous conduction mode. Secondary rectification diodes are turned off with high d*i*/d*t*. This causes reverse recovery problems. In [18], SRC topology is investigated to charge a 51.2 V Li-ion battery pack. Synchronous rectifier is utilized to avoid the reverse recovery problem and to reduce the conduction losses from the diode rectifier. However, synchronous rectification also

978-1-4673-6741-7/15/$31.00 ©2015 IEEE

brings problems such as a) complicate control and addition driving circuits, b) driving losses, and c) switching losses from the secondary power MOSFETs.

On the other hand, PRC, LCC, and LLC converters have excellent voltage regulation performance in high load condition. However, all of them suffer from high circulating energy in the resonant tank. Among them, LLC converter has the lowest circulating losses and has been investigated by lots of peer researchers. However, its circulating power is still much higher than that of SRC converter. In light load condition, majority of the circulating power comes from the current flowing in the magnetic inductor of the transformer. This current flow back and forth within the transformer and does not contribute to the power delivered to the load side. This is determined by the nature of LLC topology and cannot be avoided.

This paper proposes a hybrid multi resonance dc/dc converter which is applicable to PEV battery charging application. The converter combines SRC topology with LLC topology. By putting two different resonant tanks in series, the proposed converter has the advantages of a) low circulating losses, b) good voltage regulation performance in high state of charge, and c) zero current switching for secondary diodes.

This paper is organized as follow: Circuit operations of conventional SRC and LLC topologies with load quality factor is analyzed and reviewed in Section II. In Section III, proposed hybrid SRC, LLC resonant topology is introduced and modelled. Detail operation analysis are provided. Features of proposed hybrid topology are highlighted in Section IV. A 1kW circuit prototype is designed and simulated in Section V. This paper summarizes in Section VI.

II. Circuit Operations of SRC and LLC Topologies with Low Quality Factor

A. Operation of SRC Topology

The resonant tank of SRC converter is composed of a resonant inductor L_{r1}, and a resonant capacitor C_{r1}. Resonant frequency and quality factor of SRC converter are defined in Eq. (1) and Eq. (2), respectively.

$$f_{src} = \frac{1}{2\pi\sqrt{L_{r1}C_{r1}}} \tag{1}$$

$$Q_{src} = \frac{\sqrt{L_{r1}/C_{r1}}}{n_1^2 R_{src}} \tag{2}$$

The dc gain characteristics of SRC converter associated with different quality factors are plotted in Fig. 3. Conventionally, SRC topology has mainly been investigated in inductive region ($f > f_{src}$) and high quality factor (e.g. $Q_{src} > 1$). This is because a) in telecommunication applications, the electronic load typically requires low output voltage (e.g. 12 V) and high output current, which is associated with low equivalent load resistant, R_{src}, and high quality factor; b) power MOSEFTs have ZVS features in the inductive region, which means the reverse recovery process of body diodes could be eliminated; and c) with high quality factor, SRC topology has good voltage regulation performance, so that it is able to tolerate the voltage variation from the dc link.

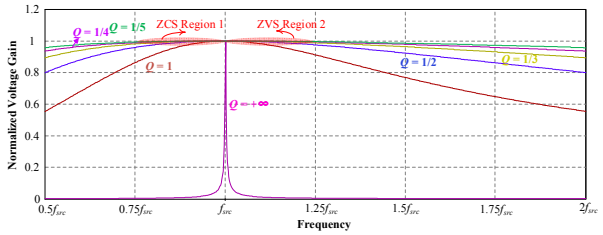

Fig. 3. Dc gain characteristics of SRC converter under different load variations.

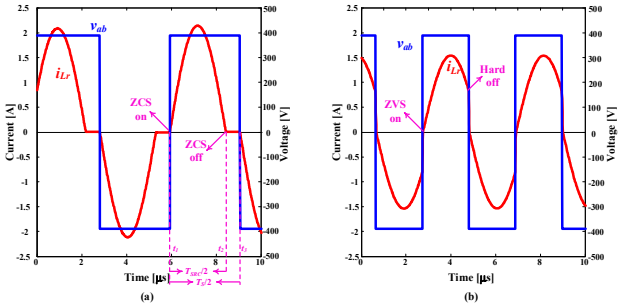

Fig. 4. Operation comparison of SRC converter in a) region 1; and b) region 2.

TABLE I
COMPARISON OF SRC TOPOLOGY OPERATING IN REGION 1 AND REGION 2

Performance	ZCS Region 1	ZVS Region 2
MOSFETs turning on	ZCS	ZVS
MOSFETs turning off	ZCS	Hard switching
Body diodes turning off	ZCS	Not activated
Conduction loss from body diodes	Yes	No
Secondary diodes turning off	ZCS	Hard switching
Voltage regulation capability	Poor	Poor

However, in PEV battery charging applications, due to the high output voltage from the battery pack, SRC topology is prone to have high equivalent load resistance, R_{src}, and low quality factor. With low quality factor, the operation of SRC topology has some special features.

The key operating waveforms of SRC converter in ZCS region 1 and ZVS region 2 (as denoted in Fig. 3) are plotted in Fig. 4. In ZVS region 2, SRC converter demonstrates ZVS turning on and hard turning off from the primary power MOSFETs, which agrees with the general operation of resonant converter in inductive region. However, in ZCS region 1, the behavior of SRC converter is rather different from the general operation of resonant converter in capacitive region.

There are three aspects of advantages for SRC topology operating in ZCS region 1. First, as can been observed in Fig. 4 (a), at t_1, MOSFET S_1 and S_4 are both turned on with ZCS; secondary diodes D_1 and D_4 are also turned on with ZCS. At t_2, S_1 and S_4 are both turned off with ZCS; secondary diodes D_1 and D_4 are also turned off with ZCS. This means zero switching loss from both the primary and secondary sides. Secondly, the body diodes of power MOSFETs never conduct in this whole process. In comparison to the operation in ZVS region 2, the conduction losses caused by the voltage

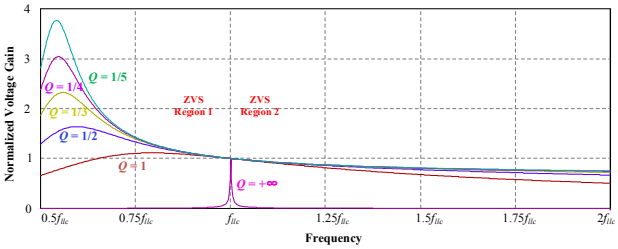

Fig. 5. Dc gain characteristics of LLC converter under different load variations.

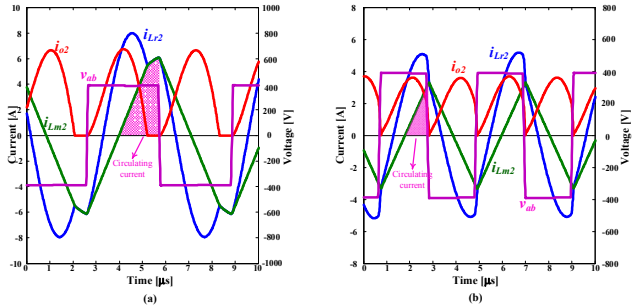

Fig. 6. Operation comparison of LLC converter in a) region 1; and b) region 2.

TABLE II
COMPARISON OF LLC TOPOLOGY OPERATING IN REGION 1 AND REGION 2

Performance	Region 1	Region 2
MOSFETs turning on	ZVS	ZVS
MOSFETs turning off	Hard switching	Hard switching
Body diodes turning off	ZCS	ZCS
Circulating losses	High	Low
Secondary diodes turning off	ZCS	Hard switching
Voltage regulation capability	Good	Poor

drop from the body diodes are totally eliminated. Thirdly, since the large magnetizing inductor has high impedance, circuiting current in magnetizing inductor is negligible. This means the circulating losses associated with the circuiting current is much smaller than that of LLC topology. Performance comparison of SRC converter operating in ZCS region 1 and ZVS region 2 is summarized in Table I.

In ZCS region 1, the main challenge of SRC topology lies its poor voltage regulation performance. As can be observed in Fig. 3, the normalized voltage is approximately unity in ZCS region 1, which makes the frequency modulation of the voltage gain infeasible.

B. Operation of LLC Topology

Fig. 6 shows the schematic of LLC resonant dc/dc converter. The resonant tank of LLC converter is composed of a resonant inductor L_{r2}, a resonant capacitor C_{r2}, and the magnetizing inductor of transformer, L_{m2}. The impedance of magnetizing inductance is much smaller than that of SRC topology and cannot be neglected. Resonant frequency between L_{r2} and C_{r2}, secondary resonant frequency between $L_{r2} + L_{m2}$ and C_{r2}, and quality factor of LLC converter are defined in equations (3-5), respectively.

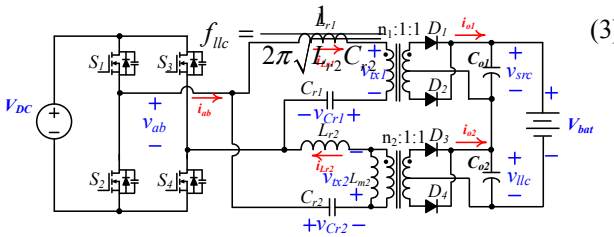

Fig. 7. Proposed hybrid SRC, LLC resonant dc/dc converter.

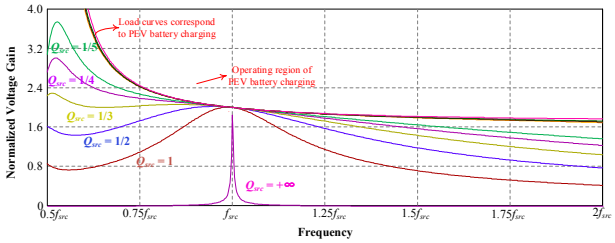

Fig. 8. Dc gain characteristics of proposed hybrid converter under different load variations.

$$f_{llc,s} = \frac{1}{2\pi\sqrt{(L_{r2} + L_{m2})C_{r2}}} \tag{4}$$

$$Q_{llc} = \frac{\sqrt{L_{r2} / C_{r2}}}{n_2^2 R_{llc}} \tag{5}$$

The dc gain characteristics of LLC converter associated with different quality factors are plotted in Fig. 5. Different from SRC, with low quality factor, LLC topology has much better voltage regulation performance.

Since LLC topology has ZVS feature in the inductive region, which is desired by the power MOSFETs, only inductive region is considered. Depending on the relationship between switching frequency and f_{llc}, the ZVS region could be divided into region 1 and region 2 (as denoted in Fig. 5). Corresponding transient operating waveforms are plotted in Fig. 6.

Advantages of LLC topology operating in ZVS region 1 lies in two aspects. First, as can been observed from Fig. 5, with the switching frequency below f_{llc}, LLC topology has good voltage regulation performance. This can be a good compensation for SRC converter. Secondly, secondary diodes are turned off with ZCS, which helps to get rid of the reverse recovery problem. This could be observed from the curve of i_{o2} in Fig. 6. However, the tradeoff is that operating in ZVS region 1 will have higher circulating losses.

Performance comparison of LLC converter operating in ZVS regions 1 and 2 is summarized in Table II. According to this comparison, ZVS region 1 is a good candidate to compensate the voltage regulation performance of SRC converter.

III. PROPOSED HYBRID SRC, LLC RESONANT DC/DC CONVERTER

A. Circuit Description

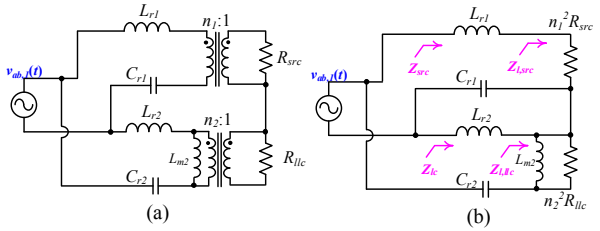

Fig. 9. Circuit model of proposed hybrid converter under FHA.

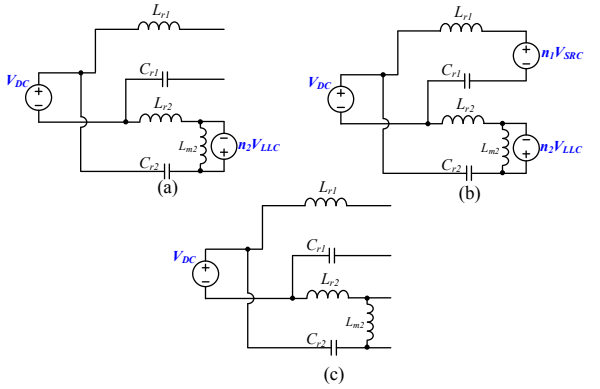

Fig. 10. Equivalent circuits during one half switching cycle; (a) mode 1; (b) mode 2; (c) mode 3.

Schematic of proposed converter is illustrated in Fig. 7. In this proposed configuration, the output of SRC topology is series with that of LLC topology; both circuits share the same full bridge inverter. SRC topology provides the base voltage, while LLC topology is utilized to provide the voltage regulation. By operating the combined resonant tank in inductive region, primary power MOSFETs will demonstrate ZVS capability.

The dc gain characteristics of proposed hybrid converter associated with different quality factors are plotted in Fig. 8. Both topologies are designed to have the same resonant frequency. According to previous comparisons, the operation zone is specified to have switching frequency smaller than the resonant frequency. As demonstrated in Fig. 8, the load curves associated with high voltage PEV battery charging have small quality factor. On one hand, this ensures that the SRC topology operates in ZCS region 1 with unity normalized voltage gain. On the other hand, the system will demonstrate good overall voltage regulation performance since LLC topology operates in ZVS region 1.

B. Circuit Modeling

Similar to the modeling of general resonant converters, modeling of proposed hybrid SRC, LLC converter is also based on first harmonic approximation (FHA) approach, which assumes that only fundamental harmonic of the square wave input is transferred to the load [19]–[23]. According to FHA, the load, low pass filter (filter capacitor), and rectifier could be modelled as an equivalent resistor, whose resistance is defined as:

$$R_{src} = \frac{8V_{src}}{\pi^2 I_{bat}} \tag{6}$$

$$R_{src} = \frac{8V_{llc}}{\pi^2 I_{bat}} = \frac{8(V_{bat} - V_{src})}{\pi^2 I_{bat}} \tag{7}$$

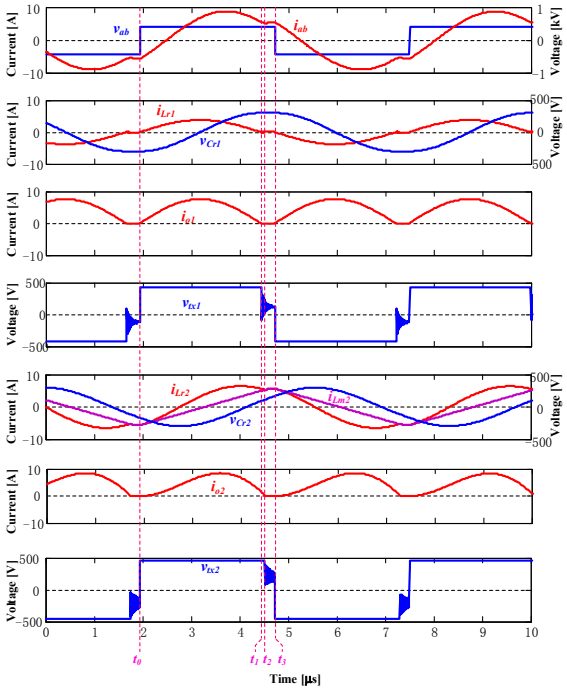

Fig. 11. Key waveforms of the proposed hybrid converter.

Circuit model of proposed hybrid converter is demonstrated in Fig. 9 (a). Resistors on the secondary side of transformer could be equivalent to the primary side; the circuit model is simplified to be Fig. 9 (b). According to Fig. 11 (b), voltage gain of the proposed circuit is obtained as,

Specifically, if the quality factor of SRC topology is small enough, the normalized voltage gain from SRC section is unity in ZCS region 1. Thus, the expression could be simplified to be:

$$G = \frac{V_{bat}}{V_{dc}} = \left| \frac{n_1^2 R_{src}}{n_1^2 R_{src} + j\omega L_{r1} + 1/j\omega C_{r1}} \right| + \left| \frac{n_2^2 R_{llc} \,||\, j\omega L_{m2}}{n_2^2 R_{llc} \,||\, j\omega L_{m2} + j\omega L_{r2} + 1/j\omega C_{r2}} \right| \tag{8}$$

$$V_{src} = \frac{V_{dc}}{n_1} \tag{9}$$

$$G = \frac{V_{bat}}{V_{dc}} = n_1 + \left| \frac{n_2^2 R_{llc} \,||\, j\omega L_{m2}}{n_2^2 R_{llc} \,||\, j\omega L_{m2} + j\omega L_{r2} + 1/j\omega C_{r2}} \right| \tag{10}$$

According to Eq. (8) and Eq. (10), the dc gain characteristic of proposed hybrid converter could be obtained.

C. Steady-state operations

Circuit operations in the first half switching cycle are symmetrical to that of the second half switching cycle. Thus, only first half switching cycle is considered. To analyze the steady-steady operations of the proposed topology, the following assumptions are made during one switching cycle.

1) The output filter capacitors, C_{o1} and C_{o2}, are large enough to assume that the output voltage V_{bat} is constant and ripple free.

2) Input voltage V_{dc} is constant and ripple free.

3) The magnetic inductor of SRC transformer has very large impedance, so that no current is associated with it.

4) Internal series resistances of passive components, as well as the voltage drop from diodes are not taken into account for convenience in calculations.

Based on these assumptions, circuit operations in one half switching cycle can be divided into three modes, which are shown in Fig. 10(a)-(c), respectively. Key waveforms of the proposed hybrid resonant converter are plotted in Fig. 11.

Mode 1, [Fig. 11(a): $t_0 < t < t_1$]:

S_2 and S_3 are turned off at t_0. This makes the operation of circuit switch to mode 1. At this moment, input current i_{ab} is still negative. i_{ab} switches conduction from S_2 & S_3 to D_{S1} & D_{S4}. Thus, input voltage v_{ab} flips from $-V_{DC}$ to V_{DC}. Since i_{Lr1} begin to increase from zero, secondary diode D_1 is turned on at zero current. Hence, SRC transformer is active with the voltage on the primary side equal to n_1V_{SRC}. Similarly, since i_{Lr2} begin to go higher than i_{Lm2}, secondary diode D_4 is turned on at zero current. Thus, the voltage on the primary side of the LLC transformer is equal to $-n_2V_{LLC}$.

From t_0 to t_1, L_{r1} and C_{r1} begin to resonate. Initial current of L_{r1} is zero. Initial voltage of C_{r1} is denoted as $V_{Cr1,0}$. Summation of voltages applied to L_{r1} and C_{r1} is equal to $V_{DC} - n_1V_{src} = 0$V. Thus, the expression of i_{Lr1} and v_{Cr1} could be solved as,

$$i_{Lr1}(t) = \frac{-V_{Cr1,0}}{Z_{src}} \sin \omega_o (t - t_0) \tag{11}$$

$$v_{Cr1}(t) = V_{Cr1,0} \cos \omega_o (t - t_0) \tag{12}$$

where ω_o is the angular resonance frequency, and Z_{src} is the characteristic impedance of SRC converter.

$$\omega_o = \frac{1}{\sqrt{L_{r1}C_{r1}}} = \frac{1}{\sqrt{L_{r2}C_{r2}}} \tag{13}$$

$$Z_{src} = \sqrt{\frac{L_{r1}}{C_{r1}}} \tag{14}$$

Similarly, L_{r2} and C_{r2} begin to resonant in mode 1. Initial current of L_{r2} is denoted as $I_{Lr2,0}$. Initial voltage of C_{r2} is denoted as $V_{Cr1,0}$. Summation of voltages applied to L_{r2} and C_{r2} is equal to $V_{dc} - n_2V_{llc}$. Thus, the expression of i_{Lr2} and v_{Cr2} could be solved as,

$$i_{Lr2}(t) = I_{Lr2,0} \cos \omega_o (t - t_0) + \frac{V_{DC} - n_2V_{llc} - V_{Cr2,0}}{Z_{llc}} \sin \omega_o (t - t_0) \tag{15}$$

$$v_{Cr2}(t) = V_{DC} - n_2V_{llc} - (V_{dc} - n_2V_{llc} - V_{Cr2,0}) \cos \omega_o (t - t_0) + Z_{llc} I_{Lr2,0} \sin \omega_o (t - t_0) \tag{16}$$

where Z_{src} is the characteristic impedance of LLC converter.

$$Z_{llc} = \sqrt{\frac{L_{r2}}{C_{r2}}} \tag{17}$$

Since constant voltage is applied to the magnetizing inductor, the current in the magnetizing inductor, i_{Lm2}, increases linearly. As defined in Eq. (18),

$$i_{Lm2}(t) = I_{Lr2,0} + \frac{n_2V_{llc}}{L_{Lm2}} (t - t_0) \tag{18}$$

In mode 1, i_{ab} increases from negative value and reaches zero at some time point. At this moment, i_{ab} switches its conduction from D_{S1} and D_{S4} to S_1 and S_4. D_{S1} and D_{S4} are turned off with ZCS; S_1 and S_4 are turned on with ZVS.

Mode 2, [Fig. 11(b): $t_1 < t < t_2$]:

At t_1, i_{Lr1} reaches zero again. According to Eq. (11) and Eq. (12), we have,

$$i_{Lr1}(t_1) = \frac{-V_{Cr1,0}}{Z_{src}} \sin \omega_o (t_1 - t_0) = 0 \tag{19}$$

$$t_1 - t_0 = \frac{\pi}{\omega_o} \tag{20}$$

$$v_{Cr1}(t_1) = V_{Cr1,0} \cos \omega_o (t_1 - t_0) = -V_{Cr1,0} \tag{21}$$

Eq. (20) shows the length of mode 1 is equal to half of the resonant period. Secondary side diode D_1 are turned off with ZCS. Since $V_{dc} - v_{Cr1}(t_1) - v_{Lr1}(t_1) \le V_{SRC}$, D_2 is also disabled. Thus, the SRC transformer is disabled and is equivalent to an open circuit. L_{r1} does not resonate with C_{r1} in mode 2. i_{Lr1} is kept to be zero, and v_{Cr1} is kept as a constant voltage.

According to the law of energy conservation, we have,

$$\int_{t_0}^{t_1} i_{Lr1}(t) V_{dc} dt = \int_{t_0}^{t_1} i_o(t) V_{src} dt \tag{22}$$

According to the principle of transformer, we have

$$i_{Lr1}(t) = \frac{i_o(t)}{n_1} \tag{23}$$

Combing Eq. (22) and Eq. (23), we have,

$$V_{dc} = n_1 V_{src} \tag{24}$$

This well explains why the normalized voltage gain of SRC topology is equal to unity with small quality factor in ZCS region 1.

In mode 2, the operation of LLC converter still follows the operation in mode 1 as defined by equations (15-18).

Mode 3, [Fig. 11(c): $t_2 < t < t_3$]:

SRC transformer is still disabled. Thus, i_{Lr1} is still kept to be zero, while v_{Cr1} is kept to be a constant voltage. At t_2, i_{Lr2} intersects with i_{Lm2}; secondary diode D_4 is turned off with ZCS. Since $V_{dc} - v_{Cr2}(t_2) - v_{Lr2}(t_2) \le V_{LLC}$, LLC transformer is disabled and the circuit enters into mode 3. Magnetizing inductor L_{m2} begins to participate into the resonance with L_{r2} and C_{r2}. The equivalent circuit is plotted as Fig. 11(c).

Initial current $i_{Lr2}(t_2)$ is denoted as $I_{Lr2,2}$; initial voltage $v_{Cr2}(t_2)$ is denoted as $V_{Lr2,2}$. Thus, the expression of i_{Lr2}, i_{Lm2}, and v_{Cr2} could be obtained as,

$$i_{Lr2}(t) = i_{Lm2}(t) = I_{Lr2,2} \cos \omega_{o,2} (t - t_2) + \frac{V_{dc} - V_{Cr2,2}}{Z_{llc,2}} \sin \omega_{o,2} (t - t_2) \tag{25}$$

$$v_{Cr2}(t) = V_{dc} - (V_{dc} - V_{Cr2,2}) \cos \omega_{o,2} (t - t_2) + Z_{llc,2} I_{Lr2,2} \sin \omega_{o,2} (t - t_2) \tag{26}$$

where $\omega_{o,2}$ is the secondary angular resonance frequency, and $Z_{llc.2}$ is the secondary characteristic impedance of LLC converter.

$$\omega_{o,2} = \frac{1}{\sqrt{(L_{r2} + L_{Lm2})C_{r2}}} \tag{27}$$

$$Z_{llc.2} = \sqrt{\frac{L_{r2} + L_{Lm2}}{C_{r2}}} \tag{28}$$

At t_3, S_1 and S_4 are turned off. Input current i_{ab} switches its conduction from S_1 & S_4 to D_{S2} & D_{S3}. Thus, input voltage v_{ab} flips from V_{dc} to $-V_{dc}$, and the circuit enters into the next half switching cycle. Both S_1 and S_4 are turned off with hard switching, and the turn off current is equal to the $i_{Lr2}(t_3)$.

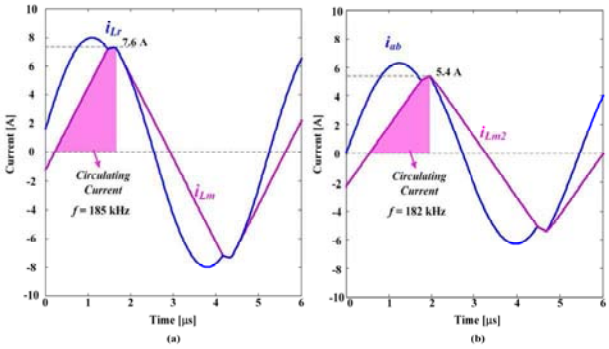

Fig. 12. Performance comparison at the maximum power point (420 V, 2.38A); a) conventional LLC topology; b) proposed hybrid topology.

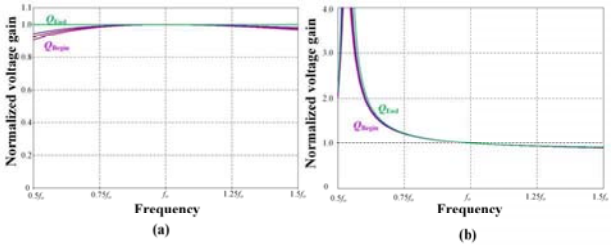

Fig. 13. Comparison of dc voltage gain characteristics in PEV battery charging application; a) conventional SRC topology; b) proposed hybrid topology.

TABLE III
DESIGN OF A 1 KW HYBRID SRC, LLC CONVERTER

Symbol	Quantity or Device	Parameter
V_{dc}	DC link Voltage	390V
P_{max}	Rated maximum power	1 kW
f_p	Primary resonant frequency	200 kHz
T	Resonant period	5 μs
$C_{oss,eq}$	Equivalent output capacitance of MOSFET	435 pF
t_{dead}	Deadband time	150 ns
n_1	SRC transformer turn ratio	2.167:1
L_{r1}	SRC resonant inductor	63.4 μH
C_{r1}	SRC resonant capacitor	10 nF
C_{o1}	SRC filter capacitor	20 μF
n_2	LLC transformer turn ratio	2.167:1
L_{m2}	LLC magnetizing inductor	80 μH
L_{r2}	LLC resonant inductor	31.7 μH
C_{r2}	LLC resonant capacitor	20 nF
C_{o2}	LLC filter capacitor	20 μF

IV. MAIN FEATURES OF THE PROPOSED HYBRID SRC, LLC RESONANT DC/DC CONVERTER

Similar to conventional resonant topologies, the proposed hybrid SRC, LLC resonant topology has ZVS features over the whole load ranges. In comparison to LLC topology, the turning off current of MOSFETs is reduced. This is because a large portion of the power is shared by the SRC topology. The SRC topology operates in discontinuous conduction mode and does not contribute to the turning off current. Reduction of the turning off current helps to reduce the switching losses of the converter.

Secondly, the circulating current in the magnetizing inductor is also reduced, so that the conduction losses are reduced. This is because the SRC topology does not contribute to any circulating current.

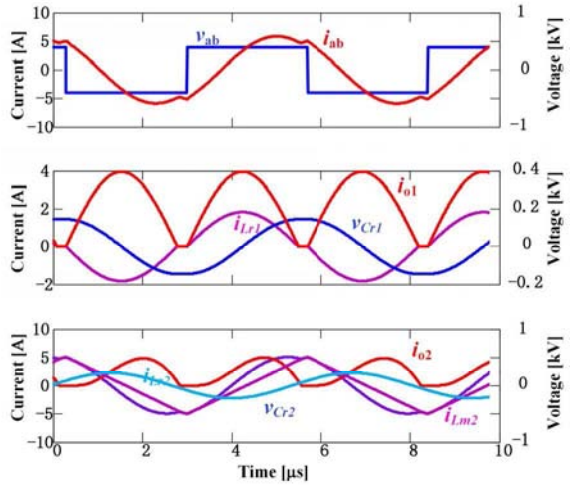

Fig. 14. Simulation waveforms at P = 856 W, Vo = 360 V.

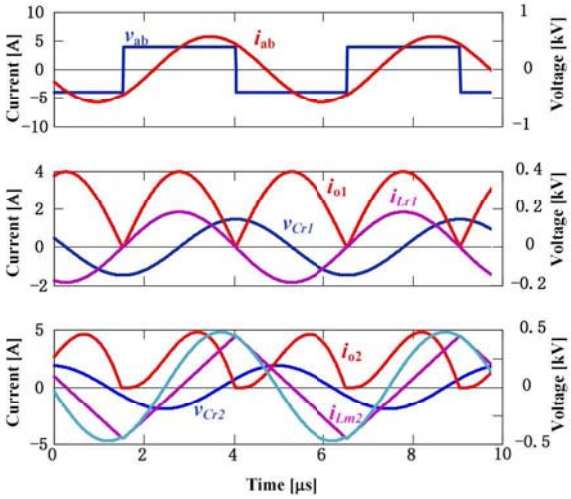

Fig. 15. Simulation waveforms at P = 928 W, Vo = 390 V.

Thirdly, the peak current of the MOSFET is reduced. In operation mode 2, the input current i_{ab} could be expressed as,

$$i_{ab}(t) = i_{Lr1}(t) + i_{Lr2}(t) = I_{Lr2,0}\cos\omega_o(t-t_0) + \frac{V_{dc} - n_2V_{llc} - V_{Cr2,0} - V_{Cr1,0}}{Z_{src}}\sin\omega_o(t-t_0) \quad (29)$$

The peak current could be calculated as,

$$I_{ab,peak} = \sqrt{I_{Lr2,0}^2 + \left(\frac{V_{dc} - n_2V_{llc} - V_{Cr2,0} - V_{Cr1,0}}{Z_{src}}\right)^2} \quad (30)$$

Generally, due to the existence of SRC topology, the current delivered to the load side is increased over the operation mode 1. With the same power level, the peak current of the MOSFET could be reduced. Reduced peak current of the MOSFET provide convenience in selecting the power devices and helps to reduce the conduction losses.

Fig. 12 shows the simulated waveforms of a conventional LLC battery charger and the proposed hybrid SRC, LLC battery charger. Both circuit are operating at the turning point of the charging process and rated at 1 kW. As demonstrated in the figure, the turning off current, circulating current, and the peak current of the MOSFET are all reduced in the proposed topology.

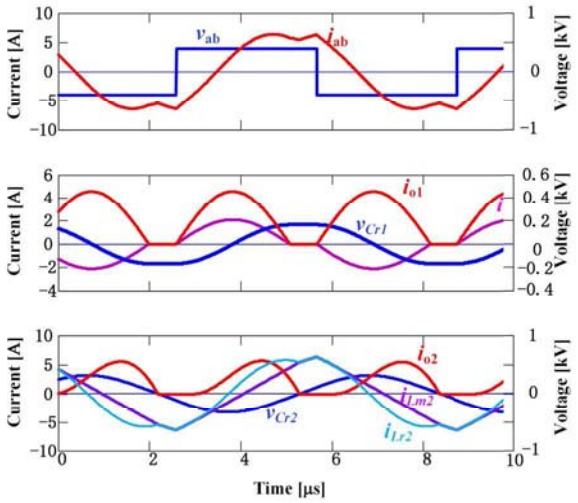

Fig. 16. Simulation waveforms at P = 1 kW, V_o = 420 V.

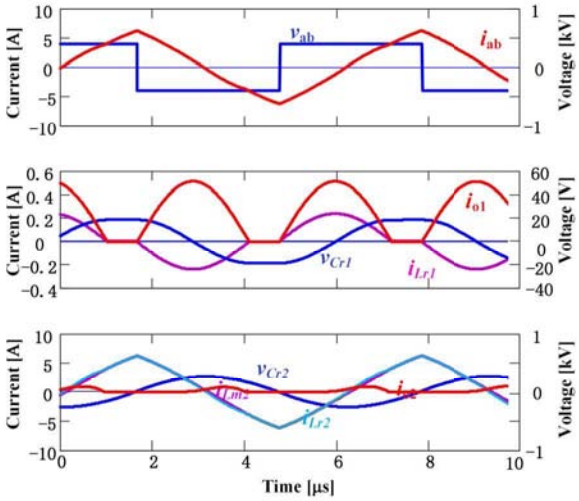

Fig. 17. Simulation waveforms at P = 100 W, V_o = 420 V.

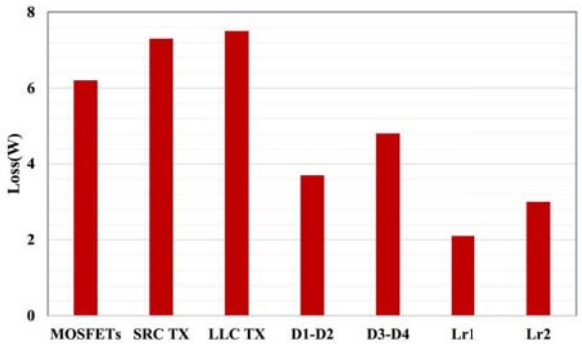

Fig. 18. Loss estimation at 1 kW operation.

Last but not least, in comparison to the SRC topology, the voltage regulation performance of the proposed converter is significantly improved. Fig. 13 shows the dc characteristic of a conventional SRC battery charger and the proposed hybrid SRC, LLC battery charger. The SRC stage in both circuits are designed to have the same resonant inductor and capacitor. As demonstrated in the figure, the proposed topology has much better voltage regulation performance.

V. Simulation Results

A 1 kW charger prototype circuit is designed and simulated. The designed parameters are summarized in Table III.

Figures 14-17 show the simulated waveforms of v_{ab}, i_{ab}, i_{o1}, v_{Cr1}, i_{Lr1}, i_{o2}, v_{Cr2}, i_{Lr2}, i_{Lm2} for four different operation conditions: P_o = 856 W, V_o = 360 V; P_o = 928 W, V_o = 390 V; P_o = 1kW, V_o = 420V; P_o = 100 W, V_o = 420V. In all those operation conditions, input current i_{ab} leads the input voltage v_{ab}, which ensures that the circuit operate in ZVS region. Since both the body diodes and the secondary diodes are turned off with ZCS, no reverse recovery process is associated with any of the didoes. The designed 1kW prototype demonstrates 96.8% peak efficiency in simulation. Fig. 18 shows the loss breakdown for different devices at output voltage of 420 V and 1 kW load condition. As shown in the figure, the losses of MOSFETs, and transformers are the dominant losses.

Independent on the change of operation points, the output voltage of SRC stage is constantly regulated to be 175 V. This means more than 40% of the total power is contributed by the SRC stage. This share of power helps reduce the circuiting current and the turning off current of the circuit. On the other hand, LLC stage is in charge of the voltage regulation.

VI. Conclusion

In this paper, SRC topology is investigated with low quality factor in high voltage PEV battery charging applications. It is found SRC circuit has unity normalized voltage gain, zero switching losses, and minimum circulating current when operating in ZCS region 1. Taking advantage of these features, a hybrid ZVS resonant topology is proposed in this paper. In the proposed hybrid topology, SRC stage is utilized to provide the base voltage; while LLC stage is employed to provide the voltage regulation.

With this proposed hybrid topology, the circulating current in the magnetizing inductor is reduced, which helps to reduce the circulating losses. The peak current of primary MOSFETs are also reduced in comparison to the conventional LLC topology; this reduces the conduction losses from the MOSFETs and improves the circuit reliability. Moreover, turning off current of power MOSFETs are reduced, which reduces the switching losses associated with the turning off of MOSFETs. Simulation results based on designed 1 kW prototype shows 96.8% peak conversion efficiency.

References

[1] W. Feng, F. C. Lee, P. Mattavelli, and D. Huang, "A Universal Adaptive Driving Scheme for Synchronous Rectification in LLC Resonant Converters," *IEEE Trans. Power Electron.*, vol. 27, no. 8, pp. 3775–3781, Aug. 2012.

[2] W. Feng, P. Mattavelli, F. C. Lee, and D. Fu, "LLC Converters with Automatic Resonant Frequency Tracking Based on Synchronous Rectifier (SR) Gate Driving Signals," in *2011 Twenty-Sixth Annual IEEE Applied Power Electronics Conference and Exposition (APEC)*, 2011, pp. 1–5.

[3] K.-H. Yi and G.-W. Moon, "Novel Two-Phase Interleaved LLC Series-Resonant Converter Using a Phase of the Resonant Capacitor," *IEEE Trans. Ind. Electron.*, vol. 56, no. 5, pp. 1815–1819, May 2009.

[4] H. Wang, S. Dusmez, and A. Khaligh, “Design and Analysis of a Full Bridge LLC Based PEV Charger Optimized for Wide Battery Voltage Range,” *IEEE Trans. Veh. Technol.*, vol. 63, no. 4, pp. 1603–1613, 2014.
[5] A. C. Sanchez, N. L. Diaz, H. R. Chamorro, and J. F. Bayona, “A Novel Analysis and Design Assessment for Series Resonant Converters Operating Above Resonance,” in *2012 10th IEEE/IAS International Conference on Industry Applications*, 2012, pp. 1–6.
[6] D. Erickson, R.W. and Maksimovic, *Fundamentals of Power Electronics*. Springer, 2001.
[7] B.-C. Kim, K.-B. Park, C.-E. Kim, B.-H. Lee, and G.-W. Moon, “LLC Resonant Converter With Adaptive Link-Voltage Variation for a High-Power-Density Adapter,” *IEEE Trans. Power Electron.*, vol. 25, no. 9, pp. 2248–2252, Sep. 2010.
[8] H. Wang, S. Dusmez, and A. Khaligh, “Maximum Efficiency Point Tracking Technique for LLC-Based PEV Chargers Through Variable DC Link Control,” *IEEE Trans. Ind. Electron.*, vol. 61, no. 11, pp. 6041–6049, Nov. 2014.
[9] F. Musavi, M. Craciun, M. Edington, W. Eberle, and W. G. Dunford, “Practical Design Considerations for a LLC Multi-resonant DC-DC Converter in Battery Charging Applications,” in *IEEE Applied Power Electronics Conference and Exposition*, 2012, pp. 2596–2602.
[10] H. Wang, A. Hasanzadeh, and A. Khaligh, “Transportation Electrification: Conductive Charging of Electrified Vehicles,” *IEEE Electrif. Mag.*, vol. 1, no. 2, pp. 46–58, Dec. 2013.
[11] H. Wang and A. Khaligh, “Comprehensive Topological Analyses of Isolated Resonant Converters in PEV Battery Charging Applications,” in *IEEE Transportation Electrification Conference and Expo.*, 2013, pp. 1–7.
[12] J.-H. Jung, H.-S. Kim, M.-H. Ryu, and J.-W. Baek, “Design Methodology of Bidirectional CLLC Resonant Converter for High-Frequency Isolation of DC Distribution Systems,” *IEEE Trans. Power Electron.*, vol. 28, no. 4, pp. 1741–1755, Apr. 2013.
[13] B. Gu, C.-Y. Lin, B. Chen, J. Dominic, and J.-S. Lai, “Zero-Voltage-Switching PWM Resonant Full-Bridge Converter With Minimized Circulating Losses and Minimal Voltage Stresses of Bridge Rectifiers for Electric Vehicle Battery Chargers,” *IEEE Trans. Power Electron.*, vol. 28, no. 10, pp. 4657–4667, Oct. 2013.
[14] Z. Pavlović, J. A. Oliver, P. Alou, Ó. Garcia, and J. A. Cobos, “Bidirectional Dual Active Bridge Series Resonant Converter with Pulse Modulation,” in *IEEE Applied Power Electronics Conference and Exposition*, 2012, pp. 503–508.
[15] H. Krishnaswami and N. Mohan, “Three-Port Series-Resonant DC – DC Converter to Interface Renewable Energy Sources With Bidirectional Load and Energy Storage Ports,” *IEEE Trans. Power Electron.*, vol. 24, no. 10, pp. 2289–2297, 2009.
[16] X. Li and A. K. S. Bhat, “Analysis and Design of High-Frequency Isolated Dual-Bridge Series Resonant DC / DC Converter,” *IEEE Trans. Power Electron.*, vol. 25, no. 4, pp. 850–862, 2010.
[17] R. L. Steigerwald, “A Comparison of Half-bridge Resonant Converter Topologies,” *IEEE Trans. Power Electron.*, vol. 3, no. 2, pp. 174–182, Apr. 1988.
[18] C.-H. Lin, C.-M. Wang, M.-H. Hung, and M.-H. Li, “Series-resonant battery charger with synchronous rectifiers for LiFePO<inf>4</inf> battery pack,” in *2011 6th IEEE Conference on Industrial Electronics and Applications*, 2011, pp. 316–321.
[19] Y. Chen, X. Wu, Z. Qian, and W. Zhang, “Design and Optimization of a Wide Output Voltage Range LED Driver Based on LLC Resonant Topology,” in *8th International Conference on Power Electronics - ECCE Asia*, 2011, pp. 2831–2837.
[20] S. De Simone, C. Adragna, C. Spini, and G. Gattavari, “Design-oriented Steady-state Analysis of LLC Resonant Converters Based on FHA,” in *International Symposium on Power Electronics, Electrical Drives, Automation and Motion, 2006. SPEEDAM 2006.*, 2006, pp. 200–207.
[21] A. A. Aboushady, K. H. Ahmed, S. J. Finney, and B. W. Williams, “Linearized Large Signal Modeling, Analysis, and Control Design of Phase-Controlled Series-Parallel Resonant Converters Using State Feedback,” *IEEE Trans. Power Electron.*, vol. 28, no. 8, pp. 3896–3911, Aug. 2013.
[22] Jee-Hoon Jung and Joong-Gi Kwon, “Theoretical Analysis and Optimal Design of LLC Resonant Converter,” in *2007 European Conference on Power Electronics and Applications*, 2007, pp. 1–10.
[23] M. K. Kazimierczuk and D. Czarkowski, *Resonant Power Converters*, vol. 7. John Wiley & Sons, 2012.